Stress Contributions in Colloidal Suspensions: The Smooth, the Rough, and the Hairy

Bram Schroyen,[1] Chiao-Peng Hsu,[1] Lucio Isa,[1] Peter Van Puyvelde,[2] and Jan Vermant[1,*]
[1]Department of Materials, ETH Zürich, 8032 Zürich, Switzerland
[2]Department of Chemical Engineering, KU Leuven, 3001 Heverlee, Belgium

(Received 2 November 2018; revised manuscript received 18 February 2019; published 29 May 2019)

The collective properties of colloidal suspensions, including their rheology, reflect an interplay between colloidal and hydrodynamic forces. The surface characteristics of the particles play a crucial role, in particular, for applications in which interparticle distances become small, i.e., at high concentrations or in aggregates. In this Letter, we directly investigate this interplay via the linear viscoelastic response of the suspensions in the high-frequency regime, using particles with controlled surface topographies, ranging from smooth to hairy and rough particles. We focus directly on the stresses at the particle level and reveal a strong impact of the surface topography on the short-range interactions, both dissipative and elastic. As the particle topography becomes more complex, the local stresses depend on how the topography is generated. The findings in this Letter, in particular, show how changes in topography can both screen or enhance the dissipation, which can be used to engineer the properties of dense or aggregated suspensions.

DOI: 10.1103/PhysRevLett.122.218001

Even the simplest colloidal suspensions, consisting of spherical particles in a Newtonian medium, display very rich and often nonlinear collective properties, e.g., concerning their diffusion, rheology, and sedimentation. For example, viscosity may vary over orders of magnitude with increasing volume fraction, and, in the same suspension, shear thinning and shear thickening can occur. These phenomena arise because of a complex interplay between colloidal and hydrodynamic interactions. Much has been learned from the simplest case of Brownian hard-sphere suspensions, mapping the behavior of more complex colloidal particles onto effective hard spheres [1,2]. Recently, however, there has been a focus on how topographical surface characteristics affect the collective properties of suspensions. For example, the influence of surface roughness and friction on discontinuous shear thickening has been the subject of several recent studies [3–8], where noncentral interactions were observed to be important. These also play a role in other properties, such as the rigidity of colloidal aggregates and gels [9–12].

Several methods exist to interrogate colloidal forces, which are also suited to investigate the role of surface topography. Single-particle measurements, e.g., using colloidal probe AFM or optical tweezers, enable direct and quantitative measurements of static interaction potentials, which can be connected to surface topography [8,13–15] or used to derive friction coefficients [8,16,17]. Yet only in special cases, e.g., by using quartz-tuning-fork AFM, dynamic effects could be probed, albeit only at a single frequency [18]. The collective properties and their volume-fraction dependency offer another approach to study particle-induced forces and their effects. For instance, the osmotic pressure [19] or linear viscoelastic properties can be used to measure the colloidal pair potential [20–24]. Rheological data have been applied to determine particle-level friction coefficients [7,25]. However, the effect of surface topography on both hydrodynamic and colloidal forces has escaped detailed analysis, while this interplay is at the heart of several important problems in dense colloidal dispersions.

In this Letter, high-frequency (HF) linear rheology is used to evaluate this interplay through a collective property. We use the volume-fraction and frequency dependency of the viscous and elastic moduli to evaluate if and how hydrodynamic forces are altered by complex topographic surfaces, e.g., for rough and hairy particles. Conceptually, the total deviatoric stress tensor in a suspension $\boldsymbol{\Sigma}$ can be written as [26–28]

$$\boldsymbol{\Sigma} = 2\eta\dot{\boldsymbol{\epsilon}} + \boldsymbol{\Sigma}_p = 2\eta\dot{\boldsymbol{\epsilon}} + (\boldsymbol{\Sigma}^H + \boldsymbol{\Sigma}^B + \boldsymbol{\Sigma}^P). \quad (1)$$

Here, $\dot{\boldsymbol{\epsilon}}$ is the bulk strain-rate tensor so that $2\eta\dot{\boldsymbol{\epsilon}}$ represents the stress contribution from the suspending fluid. The particle contribution $\boldsymbol{\Sigma}_p$ can be further decomposed into bulk hydrodynamic ($\boldsymbol{\Sigma}^H$), Brownian-induced hydrodynamic ($\boldsymbol{\Sigma}^B$), and interparticle ($\boldsymbol{\Sigma}^P$) stresses. $\boldsymbol{\Sigma}^H$ depends only on the effective volume fraction occupied by the particles, leading to an enhanced dissipation under flow [26].

As we are interested in what happens to $\boldsymbol{\Sigma}^B$ and $\boldsymbol{\Sigma}^P$ for topographically complex particles, we experiment at frequencies that are high compared to the relaxation frequencies associated with Brownian motion in the suspensions, where $\boldsymbol{\Sigma}^B$ becomes constant. For Brownian systems, the relaxation time $\tau_{p,B}$ is [21,26,29]

$$\tau_{p,B} = \frac{6\pi\eta'_\infty a^3}{k_B T} = \frac{1}{2\pi f_{p,B}}, \tag{2}$$

with $k_B T$ the thermal energy scale, a the particle radius, and $f_{p,B}$ the characteristic frequency. Important to note is that, with an increasing frequency, smaller length scales are probed, which is exploited here: When the diffusive boundary layer of momentum transport decreases to the same size as the interparticle distance, the interplay between the hydrodynamic and interparticle stresses can be inferred from the suspension's frequency-dependent response, as will be discussed below. A homebuilt piezo shear rheometer was used together with a commercial instrument to probe the linear stress response over an extended frequency range ($f = 0.001$–2000 Hz; Supplemental Material Sec. S2 [30]) [36].

Model systems with controlled surface topographies are required. We experimented on smooth, hairy, and rough systems. PMMA particles stabilized by means of densely grafted poly-12-hydroxystearic acid (PHSA) chains were used as model particles with a controllable brush chain length [37]. The ratio of the grafted chain contour length h_c over particle core size a_c was varied from $0.007 \rightarrow 0.024 \rightarrow 0.17$ (Table S1 and Fig. S1, Supplemental Material Sec. S1.1 [30]). Details have been described elsewhere [37]. A controlled roughness was obtained by employing charge-stabilized silica colloids with tuneable asperities [8,38] (Supplemental Material Sec. S1.2 [30]). The roughness was characterized via the ratio of the mean asperity height over the mean distance between asperities, from smooth (SM) to increasingly rough (RB.4 → RB.5) (Table S2 and Fig. S2 [30]). The suspending medium was generally chosen to (a) minimize van der Waals forces and (b) increase the viscosity for an increased signal to noise ratio. We compare the suspensions via an effective volume fraction based on the bulk hydrodynamic stresses, defining ϕ_{eff} from the limiting HF viscosity $\eta'_\infty = (G''_\infty/2\pi f)$. This removes difficulties in defining the geometric volume fraction for particles with complex topography [39]. The experimentally measured $\eta'_{\text{rel},\infty} = \eta'_\infty/\eta_m$ as a function of ϕ are hence shifted horizontally to a hydrodynamic model fit [40,41], as shown in Fig. 1(a) (see Supplemental Material Secs. S3 and S4 [30] for detailed information).

Figure 1(b) illustrates typical linear viscoelastic moduli (G', G'') over an extended frequency range, here for the silica-SM suspension at $\phi_{\text{eff}} = 0.43$, obtained using small strain amplitude oscillatory rheometry (Figs. S4 and S5, Supplemental Material Sec. S3 [30] for other suspensions). Representing the data in this way is, however, ill suited to directly compare the stress contributions, as bulk hydrodynamic stresses dominate the overall response. To arrive at a better representation, the data were treated. (i) The frequency in the experiments is rescaled by the characteristic Brownian frequency: $\alpha_{p,B} = (f/f_{p,B})$. (ii) The bulk hydrodynamic stresses are subtracted from the linear

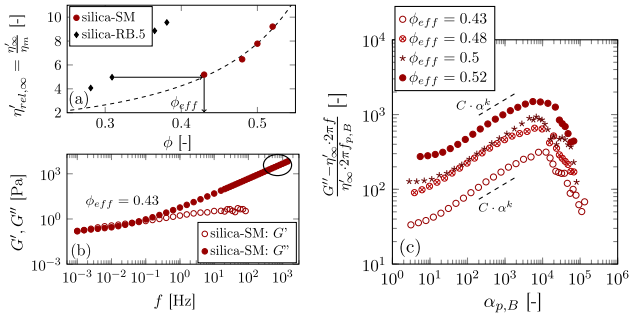

FIG. 1. (a) Determination of ϕ_{eff}, based on η'_∞, for silica-SM and -RB.5 suspensions. (b) Linear viscoelastic moduli of a silica-SM suspension at $\phi_{\text{eff}} = 0.43$. The circle indicates the limiting HF response (η'_∞). (c) Rescaling of the stresses based on the viscous response.

viscoelastic response and are used to nondimensionalize the moduli. Figure 1(c) shows the reduced viscous modulus $[(G'' - \eta'_\infty 2\pi f)/\eta'_\infty 2\pi f_{p,B}]$ for silica-SM suspensions. All suspensions displayed an intermediate regime for which the rescaled moduli increase weakly with the frequency, which was used to rescale these data further by fitting with $C\alpha^k$. In this way, we obtain reduced viscous and elastic stress amplitudes: $\Sigma_{v,r} = (1/C)(G'' - \eta'_\infty 2\pi f/\eta'_\infty 2\pi f_{p,B})$ and $\Sigma_{e,r} = (1/C)(G'/\eta'_\infty 2\pi f_{p,B})$, respectively. The different prefactors C reflect the overall interparticle interactions and are compared in Supplemental Material Sec. S5 [30] (Fig. S7). In this manner, we can directly visualize and quantify the interplay between the hydrodynamic and interparticle stresses. Two limiting cases can be considered, i.e., free draining and lubrication [26,28,42]. In the free-draining limit, hydrodynamic interactions are effectively shielded [28,43,44] and particles interact only at contact, leading to a normal-mode response with both $\Sigma_{v,r}$ and $\Sigma_{e,r}$ increasing as $\alpha_{p,B}^{1/2}$. In the lubrication limit, the thickness of the diffusive boundary layer in the HF regime decreases rapidly with the frequency $[O(\alpha_{p,B}^{-1})]$, resulting in a viscous stress which decreases with the frequency as $\Sigma_{v,r} \propto \alpha_{p,B}^{-1}$ and an elastic component that becomes constant, i.e., $\Sigma_{e,r} \propto \alpha_{p,B}^{0}$ [26]. Plots of the reduced viscous and elastic stress amplitudes versus the frequency provide direct information on how the systems behave in light of these limiting cases.

Figure 2 compares the reduced stress amplitudes for PMMA and silica suspensions, all at $\phi_{\text{eff}} \approx 0.43$. The HF regime where the slope of the reduced stress amplitudes versus the frequency changes drastically is reached only for $\alpha_{p,B} \gg 1$. Interestingly, between $\alpha_{p,B} = 1$ and these limiting regimes, the reduced stresses still increase weakly, suggesting that a single relaxation time based on Brownian self-diffusion does not capture all the dynamics of these concentrated systems. Effects from polydispersity or repulsive colloidal interactions can somewhat influence the characteristic timescales [29]. However, the weak increase

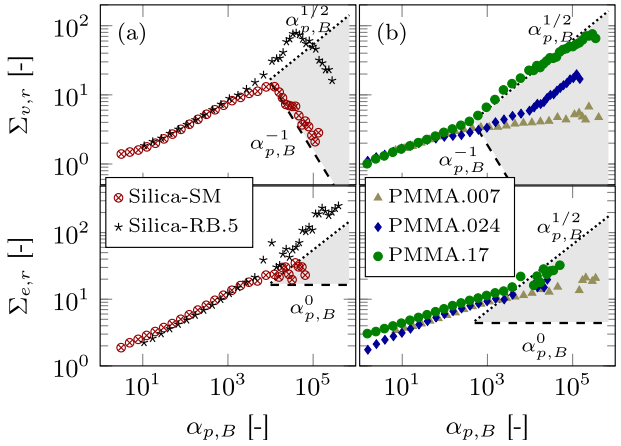

FIG. 2. Reduced viscous (top) and elastic (bottom) stress amplitudes at $\phi_{\text{eff}} \approx 0.43$. (a) Silica and (b) PMMA suspensions. The lines present the theoretical limits based on hydrodynamic lubrication (dashed) and repulsive hard-sphere (dotted) interactions, delineating the HF regime.

over several orders of magnitude in frequency suggests additional, possibly collective relaxation mechanisms [45–48].

As expected, the silica-SM suspension in Fig. 2(a) displays a lubrication scaling, consistent with earlier observations [21]: $\Sigma_{v,r}$ decreases $\propto \alpha_{p,B}^{-1}$ and $\Sigma_{e,r}$ is constant within measurement accuracy. The hairy PMMA suspensions [Fig. 2(b)] show a remarkably different asymptotic behavior, depending on the thickness of the stabilizing layer. The PMMA.007 suspension with a very thin stabilizing layer, albeit usually considered the reference model hard-sphere system [49], does not show the lubrication response expected for hard spheres and shows a weak power-law dependency. For longer grafted chain lengths, the power-law exponent increases towards the free-draining limit as the local hydrodynamic interactions become screened [28,44]. The free-draining limit is reached for the PMMA.17 suspension and possibly for the PMMA.024 at higher frequencies. Finally, for the suspension of raspberrylike silica particles [Fig. 2(a)], the behavior is drastically different. At intermediate frequencies ($\alpha_{p,B} \sim 10^4$), both $\Sigma_{v,r}$ and $\Sigma_{e,r}$ strongly increase. A lubrication regime is found only at higher frequencies compared to the smooth particles.

Varying the volume fraction helps to further interrogate the role of particle topography. For suspensions with "simple" surface topographies, such as the silica-SM suspensions in Fig. 3(a), the observed behavior is found to be independent of the volume fraction. However, for more complex topographies, the situation changes. Figure 3(b) compares the reduced stress for PMMA.17 suspensions at different ϕ_{eff} as a function of $\alpha_{p,B}$. For a constant brush geometry, the extent of hydrodynamic shielding can be

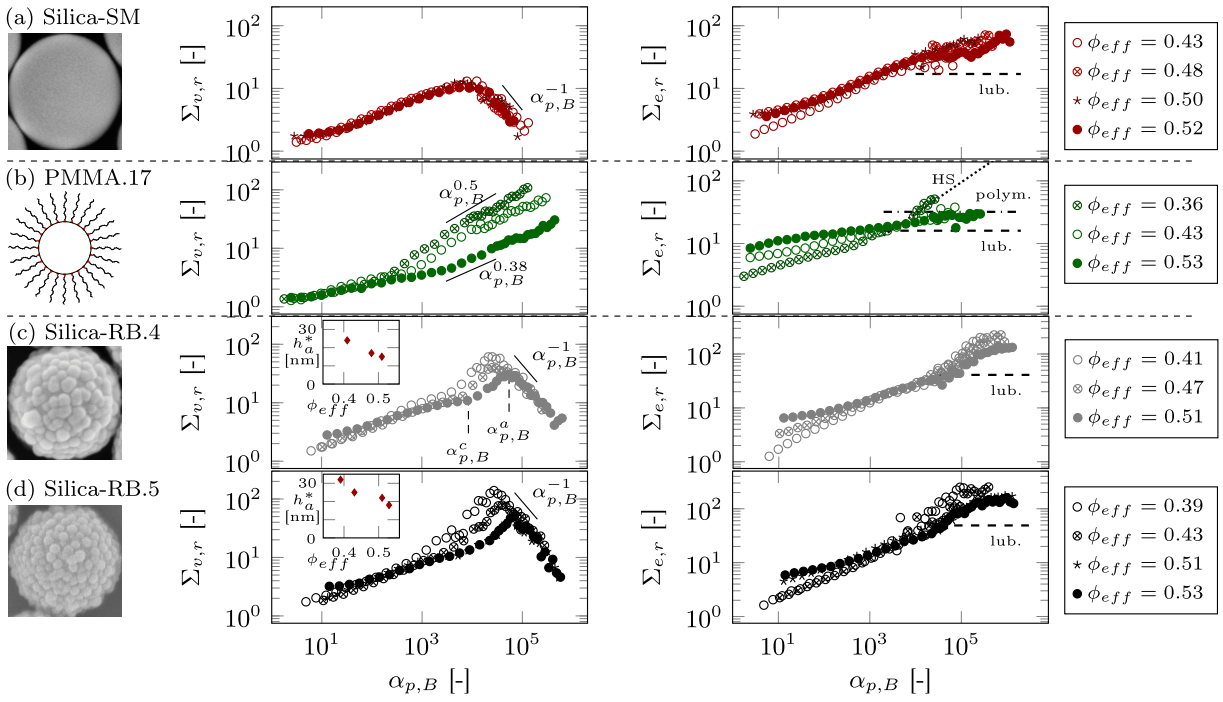

FIG. 3. Reduced viscous (left) and elastic (right) stresses as a function of the rescaled frequency for different volume fractions of (a) smooth particles, (b) particles with long polymeric brushes, and (c),(d) rough particles. (Left) The solid lines indicate the experimentally observed scaling exponents in the HF regime. $\alpha_{p,B}^{c}$ and $\alpha_{p,B}^{a}$ (c) indicate the boundaries of the intermediate regime for RB suspensions. The insets in (c),(d) show estimates of the rough layer thickness [54,55]. (Right) Dashed, dotted, and dashed-dotted lines present model predictions for $\Sigma_{e,r}$ based on lubrication [27], hard-sphere [42], and polymer-polymer interactions [56,57], respectively (Supplemental Material Sec. S6 [30]).

determined [27,43,50] and HF moduli calculated [24,51]. However, the long brushes are compressible: Figure 3(b) shows how the power-law exponent decreases with an increasing ϕ_{eff}, as upon compression of the brush an increased hydrodynamic coupling [43] is observed. Note that the viscoelastic response of the brush itself will come into play only at even higher frequencies, since the first Rouse relaxation mode of a 46PHSA strand in free suspension is expected to occur at ~50 kHz [52,53].

For the suspensions of rough silica particles [Figs. 3(c) and 3(d)], the behavior is volume-fraction dependent as well. This is more pronounced for the RB.5 compared to RB.4. The viscous stresses increase at intermediate frequencies by up to an order of magnitude compared to the smooth case, presumably due to flow inside the rough layer. The peak [$\alpha^a_{p,B}$, Fig. 3(c)] shifts to higher frequencies, and its magnitude is reduced with an increasing ϕ_{eff}. Most likely, as interparticle distances decrease further, the interpenetration becomes stronger and dissipation is reduced, as the volume where fluid flow is possible becomes smaller. At high frequencies ($\alpha_{p,B} \sim 10^5$), the $\Sigma_{v,r}$ strongly decrease as a transition to a lubrication regime is observed. The frequency at which this occurs shifts to higher values compared to the silica-SM suspensions and is higher for increased roughness. The HF regime is observed when the thickness of the diffusive layer becomes of the same order as the separation distance between the asperities on the rough surfaces of two neighboring particles.

This average separation distance δ_a can be estimated based on ϕ_{eff} using nearest-neighbor statistics [54] and varies between ~43 and 15 nm for the range studied here. The effective thickness of the rough layer is then estimated experimentally via the evolution of the diffusive boundary layer, which is $\propto a(1/\alpha_{p,B})^{1/2}$ [55], in the intermediate regime: $h^*_a \approx \frac{1}{2}\delta_a[(\alpha^a_{p,B}/\alpha^c_{p,B})^{1/2} - 1]$ [boundaries in Fig. 3(c)]. Calculated h^*_a are shown in the insets in Figs. 3(c) and 3(d). For lower ϕ_{eff}, h^*_a is of the same magnitude as the geometrical height of the asperities, which is $h_a \sim 23$ and 27 nm for the RB.4 and RB.5 suspensions, respectively (Table S2 [30]). The estimated thickness h^*_a decreases with ϕ_{eff} due to the enhanced interpenetration. This is an interesting point for future research since roughness, and its implications, can be characterized based on the rheological response.

The HF-limiting elastic stresses are easier to rationalize. Model predictions were determined by taking into account contributions from lubrication stresses [27,42], hard-sphere repulsions [42,58], or direct repulsive interactions between polymer brushes [56,57,59]. Calculations are given in Supplemental Material Sec. S6 [30]. The predicted HF-limiting stresses $\Sigma_{e,r}$, rescaled in the same manner as the experimental data, are given in Fig. 3. For the silica suspensions, plateau values based on lubrication forces only [27] underestimate the measured values due to the electrostatic repulsive interactions present. For the polymerically stabilized PMMA suspensions, the exponent of the HF elastic stress decreases with ϕ_{eff}, in line with the viscous stresses. The elastic response shifts from the scaling expected for shielded hard-sphere contacts [42] to that given by a compressed brush [51,56,57]. For the rough particles, as the lubrication regime is reached, the elastic stress also reaches a plateau. The magnitude of $\Sigma_{e,r}$ is higher than that expected for smooth spheres. However, a normal mode scaling as would be seen upon hard contacts is not observed under these equilibrium conditions.

The details of the surfaces have a very strong impact on the short-range interactions between colloids. The implications are visible in the nonlinear rheological properties as well, as shown in Supplemental Material Sec. S7 [30]: Effectively shielding the lubrication interactions by means of a polymer brush suppresses the extent of shear thickening, while surface asperities cause interlocking and strong tangential interactions, reducing the onset stress for shear thickening. Overall, it can be concluded that (i) the reference PMMA-PHSA suspensions, which are often considered to be ideal near-hard spheres based on phase diagrams, show significant screening of the hydrodynamic stresses due to the topography of the polymer brushes; (ii) polymeric brushes can be used to screen lubrication interactions, with important and interesting consequences on phenomena such as shear thickening [60–62]; and (iii) surface asperities introduce increased local dissipation, which will be important when particles come close together before hard-sphere hydrodynamic lubrication forces kick in. These findings show that topography modulates local viscous interactions, which is important for a range of phenomena in colloidal suspensions where particles approach each other at short distances. The information extracted from these quiescent measurements may give additional guidelines to design shear responses.

The authors thank L. Palangetic, R. Kalt, and G. Colombo for synthesis of the PMMA particles. J. Swan, N. Wagner, and J. Mewis are thanked for discussions. A. Studart and N. D. Spencer are thanked for access to instrumentation. We acknowledge the European Union (EU) Horizon 2020-INFRAIA-2016-1, European Soft Matter Infrastructure Grant Agreement No. 731019, SIM Flanders (SBO-TRAP), the Swiss National Science Foundation Grant No. PP00P2-172913/1, and the Eidgenössische Technische Hochschule Research Grant ETH-4916-1 for financial support.

*Corresponding author.
jan.vermant@mat.ethz.ch.

[1] W. B. Russel, D. A. Saville, and W. R. Schowalter, *Colloidal Dispersions* (Cambridge University Press, Cambridge, England, 1989).
[2] J. Mewis and N. Wagner, *Colloidal Suspension Rheology* (Cambridge University Press, Cambridge, England, 2012).

[3] D. Lootens, H. van Damme, Y. Hémar, and P. Hébraud, Dilatant Flow of Concentrated Suspensions of Rough Particles, Phys. Rev. Lett. **95**, 268302 (2005).

[4] R. Mari, R. Seto, J. F. Morris, and M. M. Denn, Discontinuous shear thickening in brownian suspensions by dynamic simulation, Proc. Natl. Acad. Sci. U.S.A. **112**, 15326 (2015).

[5] N. Y. C. Lin, B. M. Guy, M. Hermes, C. Ness, J. Sun, W. C. K. Poon, and I. Cohen, Hydrodynamic and Contact Contributions to Continuous Shear Thickening in Colloidal Suspensions, Phys. Rev. Lett. **115**, 228304 (2015).

[6] J. R. Royer, D. L. Blair, and S. D. Hudson, Rheological Signature of Frictional Interactions in Shear Thickening Suspensions, Phys. Rev. Lett. **116**, 188301 (2016).

[7] L. C. Hsiao, S. Jamali, E. Glynos, P. F. Green, R. G. Larson, and M. J. Solomon, Rheological State Diagrams for Rough Colloids in Shear Flow, Phys. Rev. Lett. **119**, 158001 (2017).

[8] C.-P. Hsu, S. N. Ramakrishna, M. Zanini, N. D. Spencer, and L. Isa, Roughness-dependent tribology effects on discontinuous shear thickening, Proc. Natl. Acad. Sci. U.S.A. **115**, 5117 (2018).

[9] G. Bossis, A. Meunier, and J. F. Brady, Hydrodynamic stress on fractal aggregates of spheres, J. Chem. Phys. **94**, 5064 (1991).

[10] J. P. Pantina and E. M. Furst, Elasticity and Critical Bending Moment of Model Colloidal Aggregates, Phys. Rev. Lett. **94**, 138301 (2005).

[11] V. Becker and H. Briesen, Tangential-force model for interactions between bonded colloidal particles, Phys. Rev. E **78**, 061404 (2008).

[12] J. Colombo and E. Del Gado, Self-assembly and cooperative dynamics of a model colloidal gel network, Soft Matter **10**, 4003 (2014).

[13] B. A. d. L. Costello, P. F. Luckham, and T. F. Tadros, Investigation of the interaction forces of polymer-coated surfaces using force balance, rheology, and osmotic pressure results, Langmuir **8**, 464 (1992).

[14] S. J. O'Shea, M. E. Welland, and T. Rayment, An atomic force microscope study of grafted polymers on mica, Langmuir **9**, 1826 (1993).

[15] G. Bryant, S. R. Williams, L. Qian, I. K. Snook, E. Perez, and F. Pincet, How hard is a colloidal "hard-sphere" interaction? Phys. Rev. E **66**, 060501(R) (2002).

[16] X. Ling, H. Butt, and M. Kappl, Quantitative measurement of friction between single microspheres by friction force microscopy, Langmuir **23**, 8392 (2007).

[17] N. Fernandez, J. Cayer-Barrioz, L. Isa, and N. D. Spencer, Direct, robust technique for the measurement of friction between microspheres, Langmuir **31**, 8809 (2015).

[18] J. Comtet, G. Chatté, A. Niguès, L. Bocquet, A. Siria, and A. Colin, Pairwise frictional profile between particles determines discontinuous shear thickening transition in non-colloidal suspensions, Nat. Commun. **8**, 15633 (2017).

[19] J. W. Goodwin, R. H. Ottewill, and A. Parentich, Compression studies on aqueous polystyrene latices, Colloid Polym. Sci. **268**, 1131 (1990).

[20] J. C. van der Werff, C. G. de Kruif, C. Blom, and J. Mellema, Linear viscoelastic behavior of dense hard-sphere dispersions, Phys. Rev. A **39**, 795 (1989).

[21] T. Shikata and D. S. Pearson, Viscoelastic behavior of concentrated spherical suspensions, J. Rheol. **38**, 601 (1994).

[22] A. T. J. M. Woutersen, J. Mellema, C. Blom, and C. G. de Kruif, Linear viscoelasticity in dispersions of adhesive hard spheres, J. Chem. Phys. **101**, 542 (1994).

[23] J. Bergenholtz, N. Willenbacher, N. J. Wagner, B. Morrison, D. van den Ende, and J. Mellema, Colloidal charge determination in concentrated liquid dispersions using torsional resonance oscillation, J. Colloid Interface Sci. **202**, 430 (1998).

[24] P. A. Nommensen, M. H. G. Duits, D. van den Ende, and J. Mellema, Elastic modulus at high frequency of polymerically stabilized suspensions, Langmuir **16**, 1902 (2000).

[25] R. Seto, R. Mari, J. F. Morris, and M. M. Denn, Discontinuous Shear Thickening of Frictional Hard-Sphere Suspensions, Phys. Rev. Lett. **111**, 218301 (2013).

[26] J. F. Brady, The rheological behavior of concentrated colloidal dispersions, J. Chem. Phys. **99**, 567 (1993).

[27] R. A. Lionberger and W. B. Russel, Microscopic theories of the rheology of stable colloidal dispersions, Adv. Chem. Phys. **111**, 399 (2000).

[28] J. W. Swan, E. M. Furst, and N. J. Wagner, The medium amplitude oscillatory shear of semi-dilute colloidal dispersions. part i: Linear response and normal stress differences, J. Rheol. **58**, 307 (2014).

[29] J. Bergenholtz, F. M. Horn, W. Richtering, N. Willenbacher, and N. J. Wagner, Relationship between short-time self-diffusion and high-frequency viscosity in charge-stabilized dispersions, Phys. Rev. E **58**, R4088 (1998).

[30] See Supplemental Material at http://link.aps.org/supplemental/10.1103/PhysRevLett.122.218001 for specific details, which includes Refs. [31–35].

[31] G. Ourieva, Instability in sterically stabilized suspensions, Ph. D. thesis, KU Leuven, 1999.

[32] Y. K. Teh, E.-J.and Leong, Y. Liu, B. C. Ong, C. C. Berndt, and S. B. Chen, Yield stress and zeta potential of washed and highly spherical oxide dispersions—Critical zeta potential and Hamaker constant, Powder Technol. **198**, 114 (2010).

[33] V. Gopalakrishnan and C. F. Zukoski, Effect of attractions on shear thickening in dense suspensions, J. Rheol. **48**, 1321 (2004).

[34] B. J. Maranzano and N. J. Wagner, The effects of interparticle interactions and particle size on reversible shear thickening: Hard-sphere colloidal dispersions, J. Rheol. **45**, 1205 (2001).

[35] J. Bergenholtz, J. F. Brady, and M. Vicic, The non-Newtonian rheology of dilute colloidal suspensions, J. Fluid Mech. **456**, 239 (2002).

[36] B. Schroyen, J. W. Swan, P. Van Puyvelde, and J. Vermant, Quantifying the dispersion quality of partially aggregated colloidal dispersions by high frequency rheology, Soft Matter **13**, 7897 (2017).

[37] L. Palangetic, K. Feldman, R. Schaller, R. Kalt, W. R. Caseri, and J. Vermant, From near hard spheres to colloidal surfboards, Faraday Discuss. **191**, 325 (2016).

[38] M. Zanini, C.-P. Hsu, T. Magrini, E. Marini, and L. Isa, Fabrication of rough colloids by heteroaggregation, Colloids Surf. A **532**, 116 (2017).

[39] W. C. K. Poon, E. R. Weeks, and C. P. Royall, On measuring colloidal volume fractions, Soft Matter **8**, 21 (2012).
[40] A. Sierou and J. F. Brady, Accelerated stokesian dynamics simulations, J. Fluid Mech. **448**, 115 (2001).
[41] Z. Cheng, J. Zhu, P. M. Chaikin, S.-E. Phan, and W. B. Russel, Nature of the divergence in low shear viscosity of colloidal hard-sphere dispersions, Phys. Rev. E **65**, 041405 (2002).
[42] R. A. Lionberger and W. B. Russel, High frequency modulus of hard sphere colloids, J. Rheol. **38**, 1885 (1994).
[43] S. L. Elliott and W. B. Russel, High frequency shear modulus of polymerically stabilized colloids, J. Rheol. **42**, 361 (1998).
[44] Z. Varga and J. W. Swan, Linear viscoelasticity of attractive colloidal dispersions, J. Rheol. **59**, 1271 (2015).
[45] C. Goldenberg, A. Tanguy, and J.-L. Barrat, Particle displacements in the elastic deformation of amorphous materials: Local fluctuations vs. non-affine field, Europhys. Lett. **80**, 16003 (2007).
[46] B. Wu, T. Iwashita, and T. Egami, Anisotropic stress correlations in two-dimensional liquids, Phys. Rev. E **91**, 032301 (2015).
[47] M. Maier, A. Zippelius, and M. Fuchs, Emergence of Long-Ranged Stress Correlations at the Liquid to Glass Transition, Phys. Rev. Lett. **119**, 265701 (2017).
[48] E. DeGiuli, Field Theory for Amorphous Solids, Phys. Rev. Lett. **121**, 118001 (2018).
[49] P. N. Pusey and W. van Megen, Phase behaviour of concentrated suspensions of nearly hard colloidal spheres, Nature (London) **320**, 340 (1986).
[50] A. A. Potanin and W. B. Russel, Hydrodynamic interaction of particles with grafted polymer brushes and applications to rheology of colloidal dispersions, Phys. Rev. E **52**, 730 (1995).
[51] M. H. G. Duits, P. A. Nommensen, D. van den Ende, and J. Mellema, High frequency elastic modulus of hairy particle dispersions in relation to their microstructure, Colloids Surf. A **183–185**, 335 (2001).
[52] P. E. Rouse, A theory of the linear viscoelastic properties of dilute solutions of coiling polymers, J. Chem. Phys. **21**, 1272 (1953).
[53] B. H. Zimm, Dynamics of polymer molecules in dilute solution: Viscoelasticity, flow birefringence and dielectric loss, J. Chem. Phys. **24**, 269 (1956).
[54] S. Torquato, Nearest-neighbor statistics for packings of hard spheres and disks, Phys. Rev. E **51**, 3170 (1995).
[55] L. G. Leal, *Advanced Transport Phenomena: Fluid Mechanics and Convective Transport Processes* (Cambridge University Press, Cambridge, England, 2007).
[56] R. Zwanzig and R. D. Mountain, High-frequency moduli of simple fluids, J. Chem. Phys. **43**, 4464 (1965).
[57] S. T. Milner, T. A. Witten, and M. E. Cates, Theory of the grafted polymer brush, Macromolecules **21**, 2610 (1988).
[58] N. F. Carnahan and K. E. Starling, Equation of state for noninteracting rigid spheres, J. Chem. Phys. **51**, 635 (1969).
[59] B. J. Maranzano and N. J. Wagner, Thermodynamic properties and rheology of sterically stabilized colloidal dispersions, Rheol. Acta **39**, 483 (2000).
[60] J. Bender and N. J. Wagner, Reversible shear thickening in monodisperse and bidisperse colloidal dispersions, J. Rheol. **40**, 899 (1996).
[61] J. Mewis and G. Biebaut, Shear thickening in steady and superposition flows effect of particle interaction forces, J. Rheol. **45**, 799 (2001).
[62] L.-N. Krishnamurthy, N. J. Wagner, and J. Mewis, Shear thickening in polymer stabilized colloidal dispersions, J. Rheol. **49**, 1347 (2005).